High-Fidelity Dynamic Neutron Imaging and Radiography for Subcritical Experiments and Other Applications

Project: LO-009-20, Year 3 of 3

Matthew S. Wallace,[1,a] Richard R. Freeman,[a] Alice M. Durand,[a] Aimee Neilsen,[a] Eimon Erfanfar,[a] Piotr Wiewior,[a] Eric Dutra,[a] Daniel Lowe,[b] Paul Manhart,[c] Stuart Baker,[c] Jeremy Bundgaard,[c] Don Max,[a] Steve Chapman,[d] Christopher Cooper,[d] Owen Drury,[d] Clement Goyon,[d] Alex Povilus,[d] Andrea Schmidt[d]

[1]wallacms@nv.doe.gov, (925) 960-2520
[a]Livermore Operations; [b]Nevada Operations; [c]New Mexico Operations; [d]Lawrence Livermore National Laboratory

This project aims to advance neutron technologies that support subcritical experiments (SCEs) and other dynamic material applications. In previous years, there were three main thrusts for this project. The first and main effort focused on imaging the source of neutrons on a dense plasma focus (DPF). The second portion focused on improving the neutron yield from a DPF. The source developed on the Nevada National Security Site (NNSS) Gemini DPF yielded ~8×10^{11} deuterium-deuterium (DD) neutrons/pulse in relatively short pulse widths of approximately 100 ns FWHM. This result paved the way for progress to deuterium-tritium (DT) neutron characterization, showing increased DT neutron yield at the NNSS Sodium DPF to 5×10^{13} and offering the possibility of using DPF neutrons for neutron radiography and fission neutrons for pinhole imaging neutron experiments (PINEX). Both the improving DPF neutron yield and Monte Carlo N-Particle (MCNP) simulation efforts for PINEX were completed by the second year of the project. However, the neutron imaging efforts continued into the third year with a renewed focus on analysis of more images and a portable imager design. This followed the testing of various optical components at both at the NNSS Gemini DPF and at the Los Alamos Neutron Science Center (LANSCE), and recording the first penumbral images of neutron emission spots from a DPF machine. This year, deconvolutions of additional neutron spot-size images were carried out for a second penumbral aperture geometry. These two apertures give matching results for the final spot size. Finally, a portable imaging system is ready for deployment to characterize the spot size for more potential neutron sources, and includes not only other DPFs but also a new Laser Ablation Z-pinch Experiment (LAZE) platform which is currently being pursued under other SDRD efforts (Wiewior 2021).

This work was done by Mission Support and Test Services, LLC, under Contract No. DE-NA0003624 with the U.S. Department of Energy, the Office of Defense Programs, and supported by the Site-Directed Research and Development Program. DOE/NV/03624--1401

Background

Challenges and Goals

A dense plasma focus (DPF) device consists of a central quasi-cylindrical anode surrounded by a cathode consisting of multiple axisymmetric rods (Figures 1 and 2). Insulating material separates the electrodes, starting at the base and extending partway up the anode. A chamber encases the electrodes and insulator and is filled with a low pressure of gas (commonly deuterium). A capacitor bank (called a Marx bank) is connected to the anode, charged, and initiates an arc between the cathode rods and the anode. The arc ionizes the gas into a plasma that lifts off the insulator and travels toward the open end of the electrodes. As the plasma sheath reaches the end, one end of its current arcs remains attached to the tips of the cathode rods, while the other end begins to "pinch" together at the central anode. The pinch becomes a narrow column of dense plasma that emits X-rays and neutrons. The entire process, from initial arc to pinch breakdown, occurs on the order of 10 μs or less.

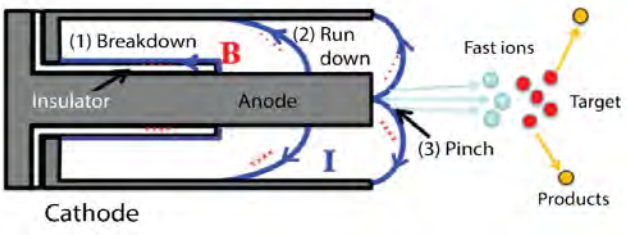

Figure 1. Diagram showing a cross section of a DPF head and the three primary stages of operation. The anode is the central cylinder, the cathode consists of a number of rods surrounding the anode, and the two are separated by an insulator; (1) is the breakdown of the gas between the two electrodes, (2) is the run-down of the plasma down the cylinder, and (3) is where the plasma converges down to a "pinch." The breakdown of the plasma radiates X-rays and produces neutrons. The directions of the magnetic field (B) and current (I) are indicated as well.

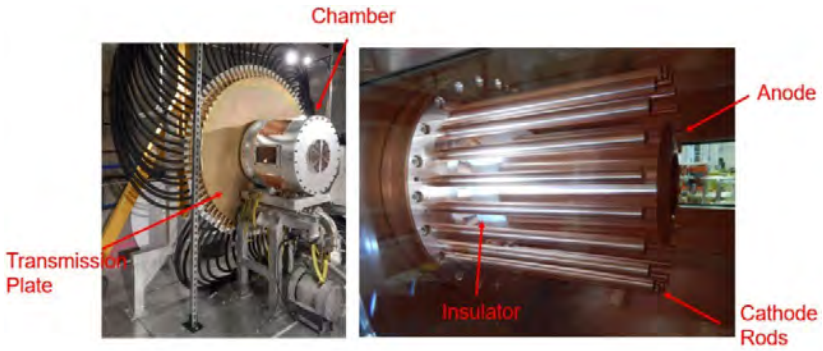

Figure 2. The MegaJOuLe Neutron Imaging Radiography (MJOLNIR) DPF at LLNL and its components.

DPF machines are a proposed diagnostic for neutron-diagnosed subcritical experiments (NDSEs) for full-scale SCEs. These fast neutron sources are also being considered as a secondary diagnostic for radiography during SCEs, as they would provide further useful constraints to the dynamic system. In general, higher neutron yields are ideal for radiography applications. In order to understand the viability of neutron radiography in this fast application, the size and shape of the source must be well characterized; but thus far there is a virtual lack of any high-quality measurements of these characteristics. Multiple mega-amp DPF devices exist within the National Nuclear Security Administration (NNSA) complex and an imaging system needs to be portable for use with these DPFs and other new types of neutron sources (Wiewior 2021).

Project

Penumbral Imaging

The previous year of penumbral imaging efforts were dedicated to the design of a penumbral aperture needed for fielding at DPF machines, and to begin development of a software package capable of image reconstruction of recorded penumbral images. To visualize how penumbral imaging works, imagine one individual point source with an isotropic neutron emission. The source shines on a detector some distance away without any apertures in between. The image formed on the detector plane will not be the same size as the point source itself—instead, the signal intensity will be spread out across the entire detector. If an aperture is inserted, it will cast a shadow of the aperture opening. This image is referred to as the point spread function (PSF) of a given aperture. Figure 3 shows an example PSF for a cylindrical aperture. See Ress for a description of the benefits of using different aperture geometries, such as a toroid (1990). If the radiation source is thought of as a collection of many individual point sources, the detector image (i.e., penumbral image) will simply be a superposition of the PSFs from each of these individual point sources.

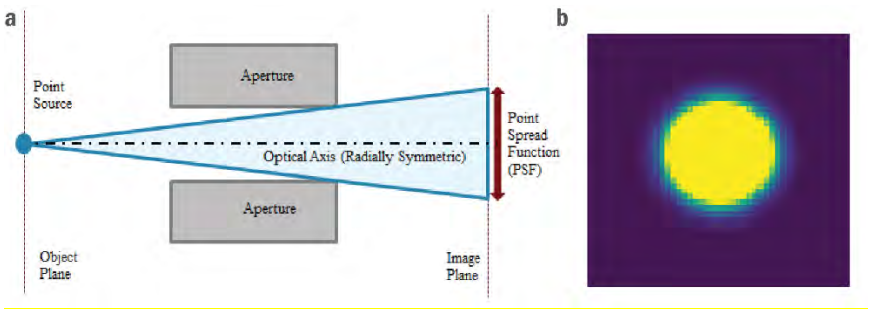

Figure 3. (a) Diagram showing a point source with signal going through a cylindrical aperture. The final image is a point spread function (PSF). (b) Example simulated PSF for a conical aperture.

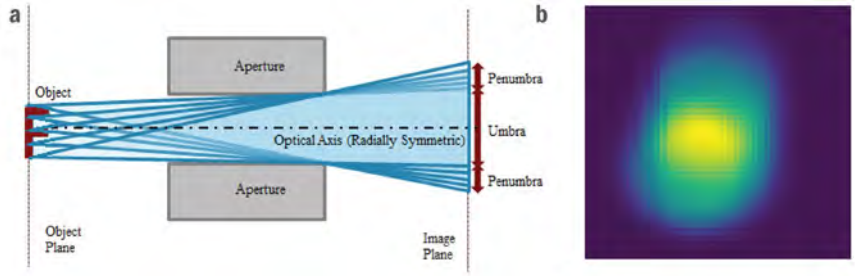

Figure 4. (a) Diagram showing an extended, F-shaped source with signal going through a cylindrical aperture. The final image is a penumbral image. (b) Example simulated penumbral image from an F-shaped source going through a conical aperture.

Figure 4 shows an example penumbral image for a conical aperture with an extended source; this case is an F-shaped source. The final image is a convolution of the source distribution with the PSF of the aperture. Previous years for this project (Durand 2020, 2021) summarize reconstruction efforts for a penumbral aperture, the design of the aperture, and testing of scintillators that were used in an early version of a neutron imaging system intended for spot size measurements and showed the first set of penumbral images on a DPF using a neutron imager.

Results

Penumbral Images of Dense Plasma Focus at Area 11

A series of penumbral images were recorded at the Area 11 DPF in January 2020. Figure 5 shows a diagram of the DPF at Area 11. The imaging system was in place at Area 11 for Radiography and Advanced Imaging Development (RAID) programmatic efforts. This source (Sodium) is described in earlier reports (Durand 2021). In the measurements described here, the DT neutrons are recorded by the imaging system after the are collimated by a 60 cm-long wall

collimator consisting of stacked layers of steel and poly. The wall collimator is embedded in the thick wall of concrete to help shield the lens and camera components in the imaging system. The imaging system consists of a scintillator, pellicle that acts as a mirror, lens, and camera. The penumbral aperture is located coaxially with the wall collimator and the neutron beam "shadow" hits the scintillator.

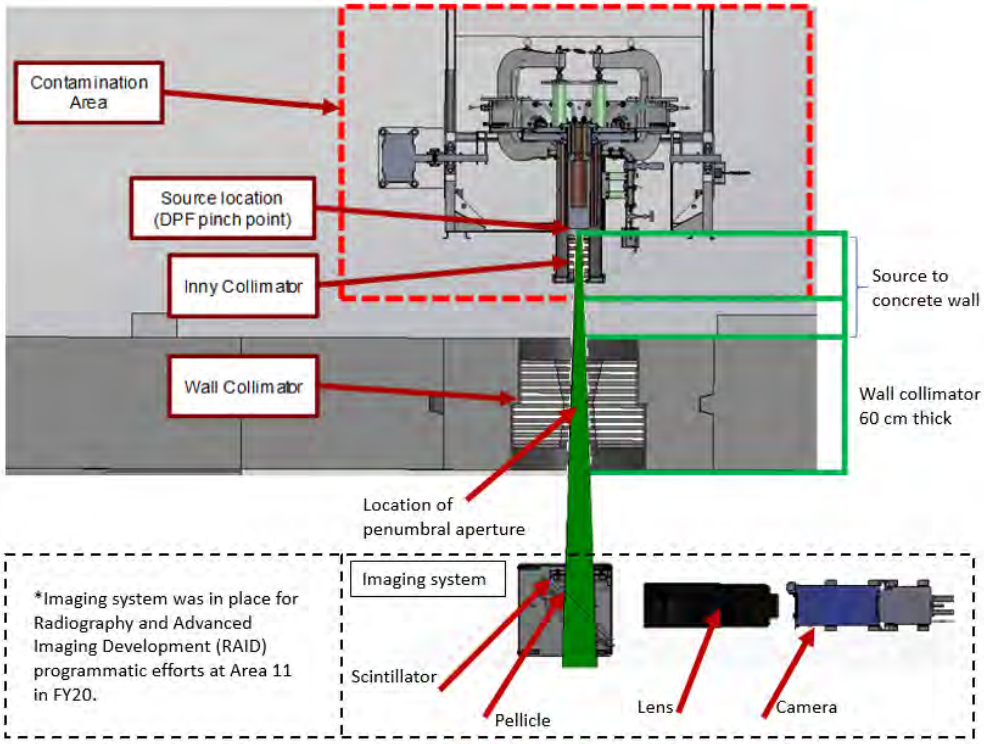

Figure 5. Schematic of the neutron imaging system in place at the Area 11 DPF. The tungsten conical penumbral aperture was in place to record a series of penumbral images to estimate the DPF spot size. The imaging system was in place at Area 11 for RAID programmatic efforts.

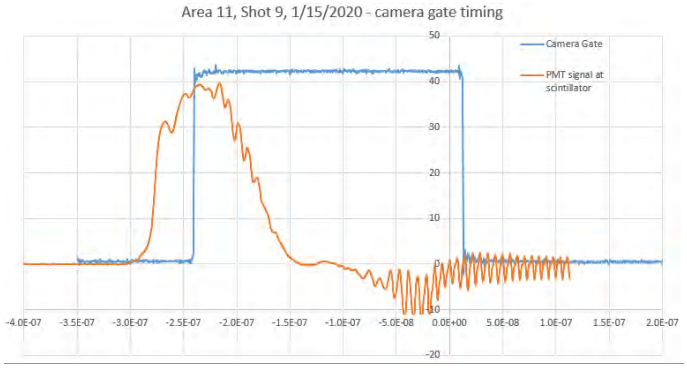

Figure 6. Example camera gate signal. The blue is the camera "on" gate and the orange is the signal from the Photomultiplier tube (PMT), which responds to both gamma-rays and neutrons. The neutron signal is not resolved from the gamma-ray, which is leading

the neutron signal by ~42 ns. The timing of the camera gate is set to suppress the recording of gamma-ray emission spots.

Figure 6 shows the camera gate superimposed on the output of a PMT placed next to the scintillator. The PMT is operated at a high gain to trigger as early as possible. This leads to saturation of the detector, so that the trace shown in Figure 6 does not accurately reflect the signal. When the DPF fires, there is generation of a large gamma-ray burst that travels at the speed of light to the detector. The gamma-rays outpace DT neutrons (14.1 MeV) generated by the DPF and arrive at the camera ~42 ns ahead of the neutrons. The gamma signal initiates the camera trigger (a 250 ns gate) which has a minimum latency time from the PMT receiving the gamma pulse equal to 47 ns. In this way, most of the gamma pulse is cut out and only the first 5 ns of the neutron pulse is missed. In the future, if the width of the gate is decreased and stepped through the approximately 100 ns neutron pulse, the time history of the spot can be investigated and unwanted background signals can be reduced.

Penumbral Apertures

In year 2, DPF spot size results from a conical aperture were presented. Figure 7 a) shows the conical aperture and its dimensions. In year 3, results from a second aperture were analyzed. Figure 7 b) shows the second aperture. This aperture, Rollin' hole, has a toroidal inner surface with an inner radius of 100 cm and a minimum diameter at the necking point of 2.54 cm.

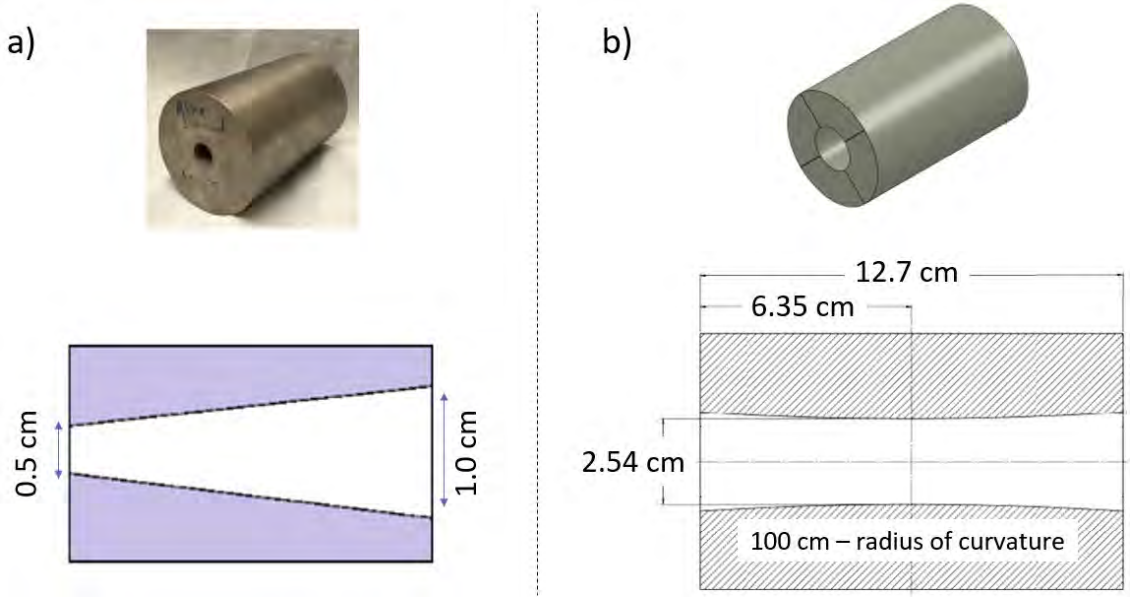

Figure 7. (a) The conical aperture used at Area 11. The aperture is a HD-18 tungsten alloy cylinder 8.2 cm long and 5.2 cm in diameter, with openings 0.5 cm and 1.0 cm in diameter. (b) The Rollin' hole aperture has a 12.7 cm long aperture with toroidal inner surface. It has a 100 cm radius of curvature for the inner surface and a 2.54 cm minimum diameter at the necking point.

Figure 8 shows unprocessed images obtained with each of the two penumbral apertures at the DPF source at Area 11. 8 a) shows the image from the conical aperture, and 8b) shows the image from the Rollin' hole aperture. The obvious difference between the two images is the diameter of the recorded circle. This of diameter difference is expected when comparing the two apertures. To process these images, the PSF for each aperture is needed and the deconvolution techniques from previous annual reports for this project can be used.

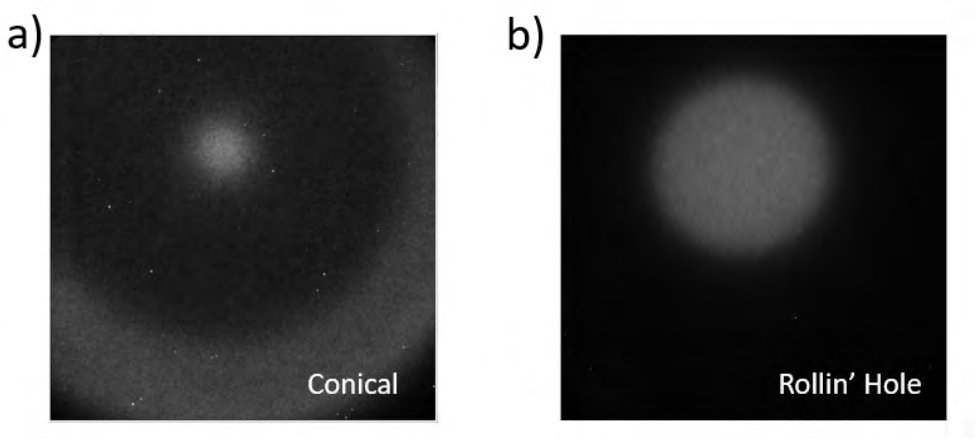

Figure 8. (a) raw image recorded using the conical aperture (b) raw image recorded using the Rollin' hole aperture.

Effect of Experimental Environment on the Point Spread Function

In order to deconvolve the "raw" images obtained on the Area 11 DPF, the point spread function (PSF) needs to be computed in our case because we do not possess a pure point source of high energy neutrons. Because a point source of high energy neutrons will partially penetrate and/or scatter from virtually any materials in the experimental hall, a detailed MCNP calculation of the PSF is required. Figure 9 shows a simplified layout of the essential elements of the imaging system up to the scintillator (called here the detector). In the figure the aperture is conical shaped and placed relative to the source and the detector plane as indicated.

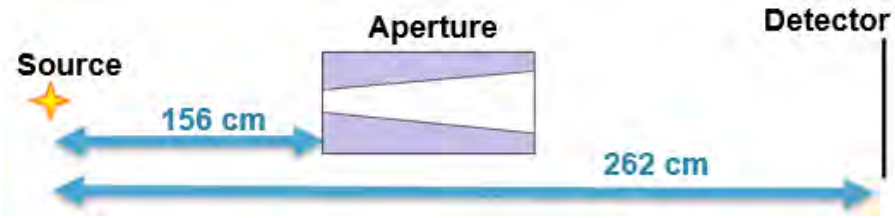

Figure 9 Simple environment which includes only the aperture in the MCNP simulation for PSF determination.

A more detailed representation of the experimental environment at Area 11 is shown in Figure 10; specifically, it includes the "inny" collimator, the concrete wall surrounding the DPF, and the wall collimator surrounding the aperture. This MCNP calculation is much more computationally intensive than the simple environment in Figure 9. Similar MCNP environments can be built up for additional laboratory spaces as the neutron imaging technique is expanded to new neutron sources.

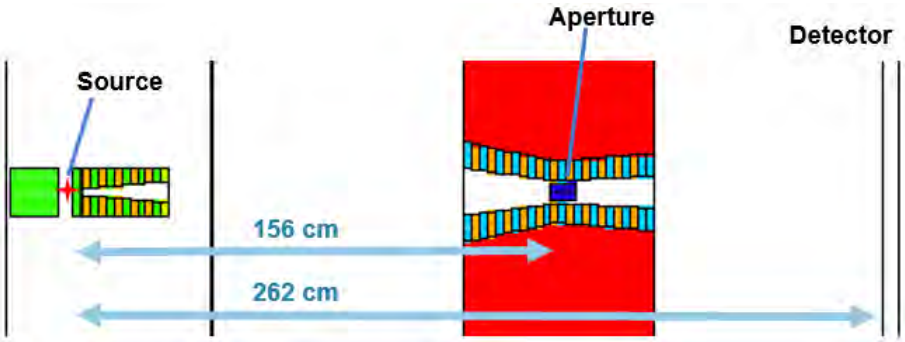

Figure 10 MCNP simulation with more complete experimental environment for more PSF determination. Environment includes the anode, inny collimator, concrete wall, wall collimator, and aperture.

Figure 11 shows lineouts across the center of the resulting two PSF calculations. The two PSF calculations differ mostly in the tails of the edges of the PSF image. Little to no difference is found in the reconstructed images obtained with the two PSF images.

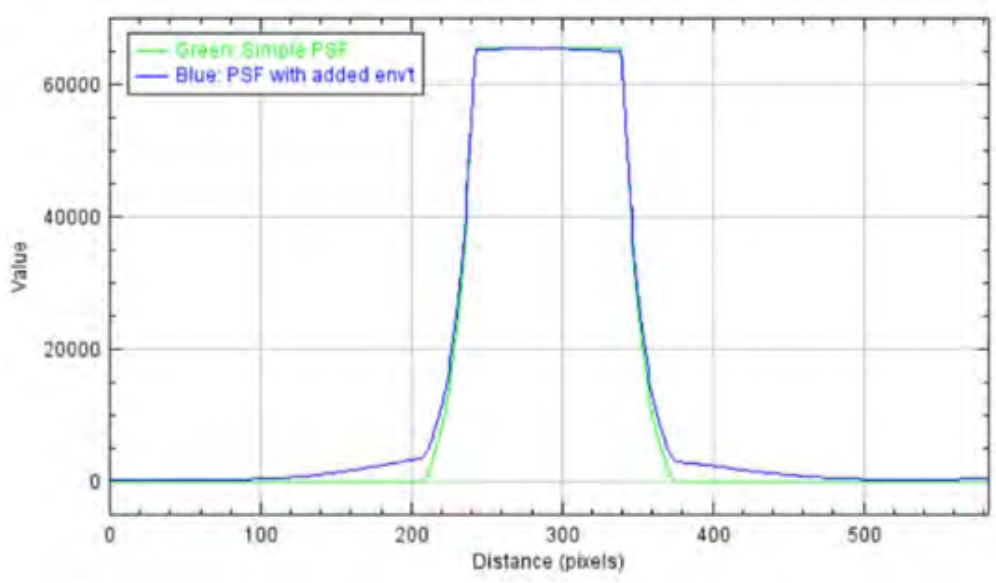

Figure 11 Lineout across the center of the two calculated PSFs from the MCNP simulations with simple environment in Figure 9 (green trace) and addition of the more complicated experimental environment from Figure 10 (blue trace). Both calculations result from the conical aperture. Little to no difference is found in the reconstructed images obtained with the two PSF images.

Effect of Optical Components on the Point Spread Function

The PSF can be further modified by blurring due to the optical components in the imaging system. Due to the finite thickness of the scintillator, the light created with in the scintillator in off axis directions leads to a blurring effect. Using Zeemax Optics studio to model this, the PSF calculated by MCNP can be convoluted to account for the scintillator and lenses in the system. Figure 12 illustrates the concept of from the imaging optics. The top portion shows a cartoon for an off-axis ray path through the scintillator and depicts the line within the scintillator where a neutron creates photons. These photons are imaged by the optics onto the detector, but only a portion of this light path is in focus. The bottom portion shows the resulting image from this single neutron ray path. Using this information and a more complete ray-trace to account for all rays that pass through the penumbral aperture, the neutron PSF can be convoluted to account for these optical effects and to refine the spot size estimates.

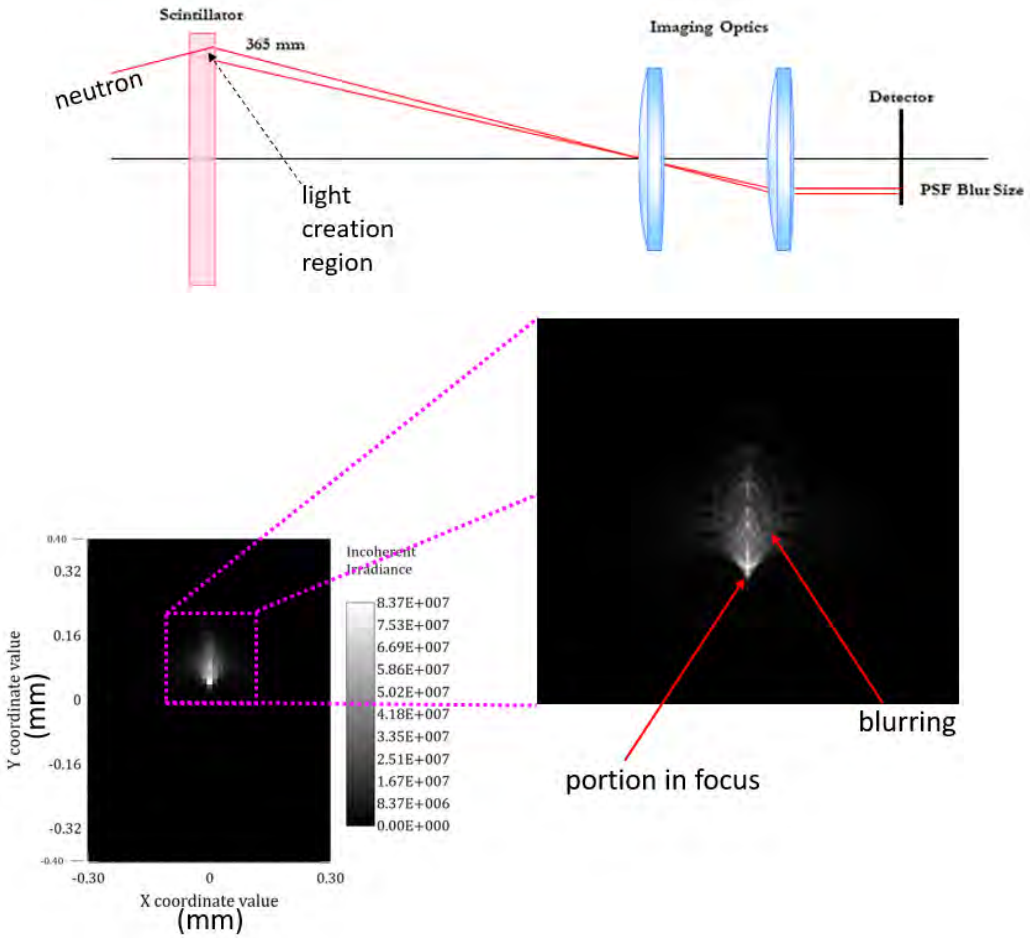

Figure 12 (Top) Cartoon of a single neutron ray-path through a scintillator and the ray paths through the imaging optics. (Bottom) Resulting image as recorded by the detector for a single neutron ray path.

DPF Neutron Spot Size Results

For each of the two apertures, PSF were determined and raw images were deconvoluted. Figure 13 shows one deconvoluted image for each of the two apertures. The horizontal red line across the middle each of the two images suggests the regions at which lineouts were taken to determine the spot sizes of the neutron sources. Figure 14 shows horizontal lineouts for three shots with each aperture (six shots total). Figure 15 shows vertical lineouts for three shots with each aperture (six shots total). Table 1 gives the measured FWHM for each of the six shots in the horizontal and vertical directions.

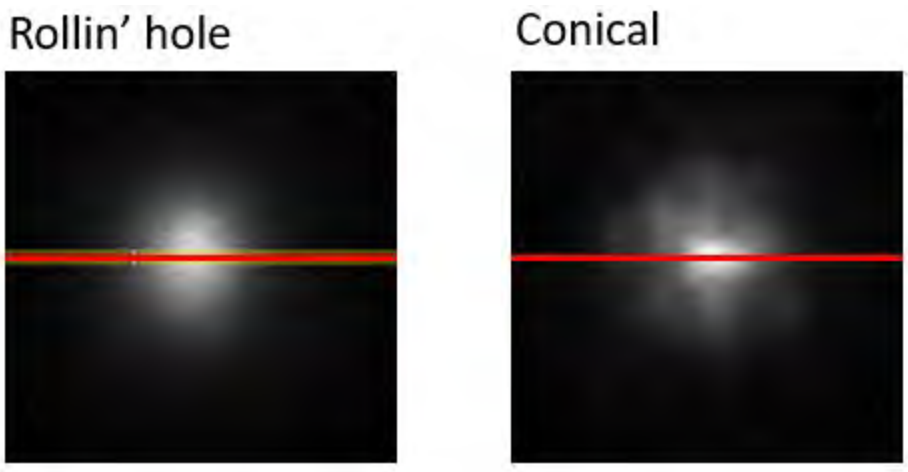

Figure 13 One deconvolved image for each of the two apertures. The red line suggests a region at which a lineout was taken to determine the FWHM of the neutron spots recorded. Figures 14 and 15 show horizontal and vertical lineouts for a total of six shots (three for each aperture type).

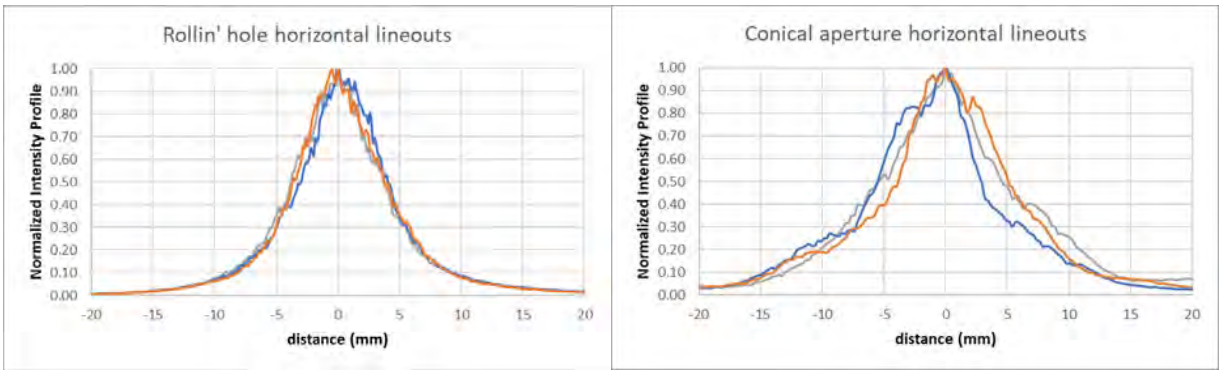

Figure 14 Horizontal lineouts for three shots with the Rollin' hole (left) and three shots with the conical (right) penumbral aperture.

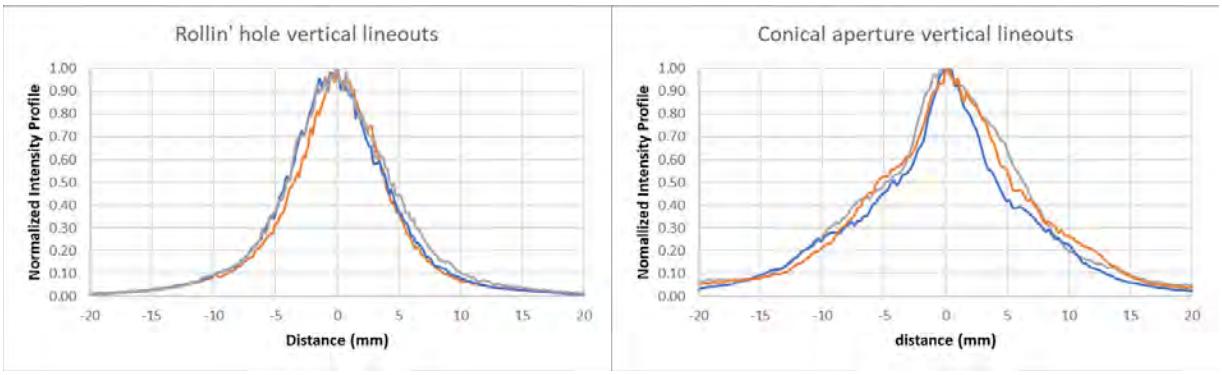

Figure 15 Vertical lineouts for three shots with the Rollin' hole (left) and three shots with the conical (right) penumbral aperture.

Aperture type	Date / time	Horiz. FWHM (mm)	Vert. FWHM (mm)
Rollin' Hole	**Jan15/11:57:13**	**7.64**	**7.40**
Rollin' Hole	**Jan15/12:27:29**	**7.03**	**8.38**
Rollin' Hole	**Jan15/12:57:12**	**7.52**	**8.26**
Conical	**Jan15/13:57:44**	**8.87**	**8.38**
Conical	**Jan15/14:26:59**	**8.38**	**10.83**
Conical	**Jan15/14/57/12**	**10.10**	**11.09**

Table 1 Recorded FWHM of the neutron spot sizes for six shots using two apertures, for the lineouts seen in Figures 14 and 15.

The spot sizes recorded with the two apertures show reasonable agreement with each other. Additional measurements (not shown here) using orthogonal rolled edges show similar horizontal and vertical spot sizes. A manuscript documenting this comparison will be submitted for publication.

Portable Imager

A neutron imaging system has been built to continue measurements of additional prospective neutron sources desired for neutron diagnosis of experiments that are of interest to the NNSS. Figure 16 shows the exploded view of the design of the imager build under this project. A portable woven-metalized tent enclosure provides electromagnetic interference (EMI) protection, and can be quickly assembled at the desired experimentation site. Figure 17 shows the folded and assembly tent enclosure and two bread boards, one holding electronics, and one holding optics fit into the enclosure. The camera optics and electronics have been set up at the Livermore Operations site.

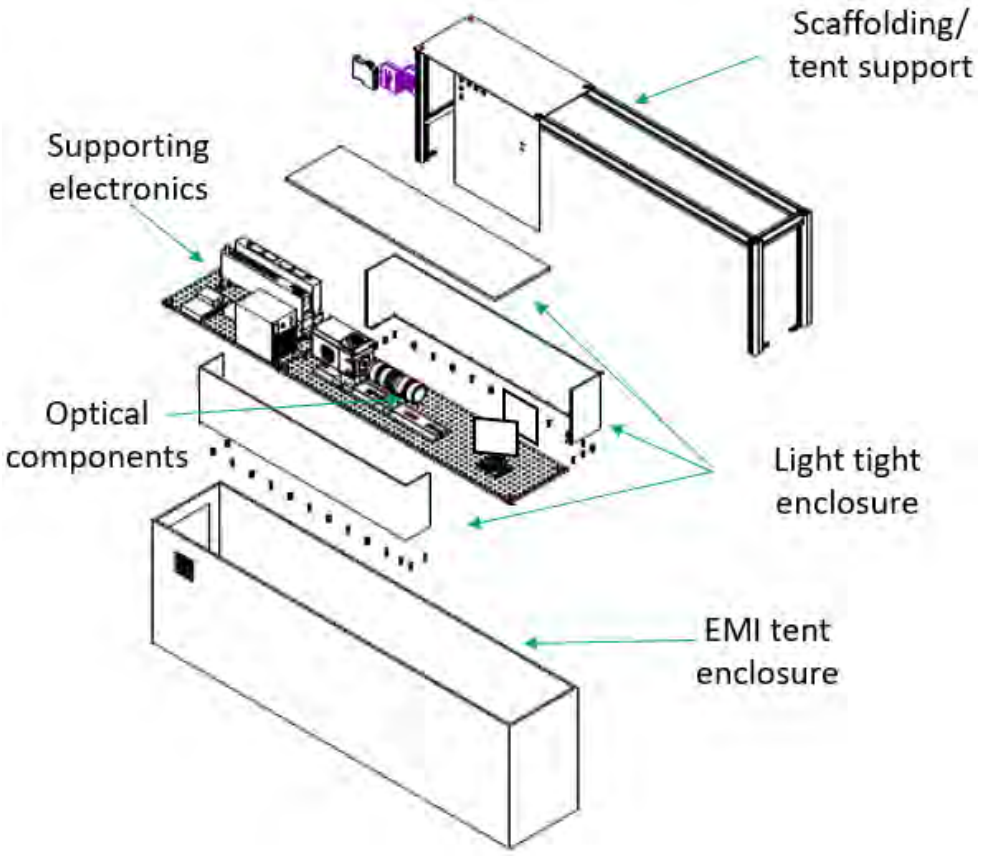

Figure 16 Exploded view of the design for the portable imaging system. The EMI enclosure (see Figure 17) houses the electrical and optical components of the neutron imaging system.

Figure 17 Portable EMI protection tent enclosure. The left picture shows the enclosure broken down. The right picture shows the erected tent enclosure being prepared for fielding on LAZE (Wiewior 2021). The enclosure allows quick assembly and two optical bread boards (one for optics and one for electronics) are placed inside.

As additional experimentation time allows, further spot size measurements will resume. These measurements include not only DPF sources, but also the LAZE source where experiments are planned to resume in the end of 2021 into 2022 (Wiewior 2021).

Conclusion

Much work was completed in the first two years. One accomplishment related to an increase in neutron flux by changing the design of the cathode and anode. An improved design for the high-yield tube resulted in DD neutron yields of ~8×10^{11} neutrons/pulse at machine parameters of 40 kV charge voltage, 2.66 MA total current, and fill pressure of 10.0 Torr. Following these results, the expected DT yield at Sodium DPF with the new HYT [High Yield Tube] is expected to be 3 to 5×10^{13} neutrons over a short (<75 ns FWHM) pulse width. The second accomplishment focused on simulating the effects of various DPF experimental configurations on the resulting neutron radiographs. A parametric study was done with neutron radiography simulations using a radiographic test object. The results from the MCNP simulations indicated that neutron radiography is feasible with the NNSS Sodium DPF and that the resultant neutron radiograph can be optimized. For the final year, all efforts under this project were spent on building the short-range neutron imager and fine-tuning the data analysis for these recorded results. Testing the imager components (scintillator, lens-coupled system, and two different cameras) demonstrated the ability to produce radiographs. Proof-of-concept experiments were performed on an X-ray source, and the source characteristics were successfully reconstructed. MCNP simulations were used to determine optimal aperture geometries, and two iterations of a penumbral aperture were fielded at a DPF. These gave agreeable results to each other. These measurements can be made more interesting by shortening the gate width of the imager and stepping the gate window through the neutron pulse. Continued experimentation is planned in the upcoming year to further these types of spot size measurements on additional types of neutron sources that are being pursued under SDRD efforts.

Significance

Development and optimization of neutron sources and imaging systems is required, as the infrastructure around many SCEs in the future will rely on pulsed neutron sources. The ability to

image an SCE in the U1a.03 drift will allow design physicists to have better fidelity when bridging the gap between experiment and simulation. Additionally, because the NDSE neutron source is the same as the neutron-imaging source, the information contained within the radiography is highly valuable. These results are of interest to design and diagnosis of new types of neutron sources being developed to further neutron science at the NNSS.

Tie to Mission/Benefit:

Neutron source, detection, and imaging system development is sought after throughout the NNSA complex.

Publications / Presentations

Results of the MCNP simulations, the neutron image processing software package, and design of the imager system were presented at summer internship poster sessions in 2019 and 2020 at NNSS and LLNL.

The deconvoluted penumbral aperture images from Area 11 were presented remotely as a part of the NNSS Science and Technology Work in Progress seminar series on July 21, 2020.

A manuscript showing the spot size measured with a penumbral aperture compared with a flat rolled edge under RAID programmatic efforts is being worked on and will be submitted for publication.

Acknowledgments

The authors thank David Fittinghoff, Scott Watson, Jim Tinsley, and Jesse Adams for their helpful discussions on reports over the duration of the project; the Sodium DPF team members for conducting shot operations at Area 11; the MJOLNIR DPF team at LLNL for useful discussions and shot operations over the duration of this project; and previous summer interns Damyn Chipman and Bryan Garcia, who have moved on to further their academic and professional careers but who were instrumental in getting this project off the ground in its early stages. The authors also thank members of the Zebra Pulsed Power Lab at the University of Nevada, Reno for preparation of fielding the neutron imager on LAZE.

References

Durand, A.M., et al. 2020. “High-Fidelity Dynamic Neutron Imaging and Radiography for Subcritical Experiments and Other Applications.” In *FY 2019 Site-Directed Research and Development Annual Report*. Las Vegas, Nevada: Mission Support and Test Services, LLC.

Durand, A.M., et al. 2021. “High-Fidelity Dynamic Neutron Imaging and Radiography for Subcritical Experiments and Other Applications” In *FY 2020 Site-Directed Research and Development Annual Report*. Las Vegas, Nevada: Mission Support and Test Services, LLC.

Ress, D. 1990. “Design of thick apertures for high-resolution neutron penumbral imaging.” *IEEE Trans. Nucl. Sci.* 37 (2):155–160.

Wiewior, P., et al. 2021. “Z-Pinch and Laser-Ablation–Driven High-Yield Neutron Source” In *FY 2020 Site-Directed Research and Development Annual Report*. Las Vegas, Nevada: Mission Support and Test Services, LLC.

Yeamans, C. B., Blue, B. E. 2017. “National Ignition Facility neutron sources.” LLNL-CONF-739397. Livermore, California: Lawrence Livermore National Laboratory. https://www.osti.gov/servlets/purl/1458648.